Cell Cycle

ISSN: 1538-4101 (Print) 1551-4005 (Online) Journal homepage: http://www.tandfonline.com/loi/kccy20

Differential binding of p53 and nutlin to MDM2 and MDMX: Computational studies

Thomas Leonard Joseph, Arumugam Madhumalar, Christopher J. Brown, David P. Lane & Chandra S. Verma

To cite this article: Thomas Leonard Joseph, Arumugam Madhumalar, Christopher J. Brown, David P. Lane & Chandra S. Verma (2010) Differential binding of p53 and nutlin to MDM2 and MDMX: Computational studies, Cell Cycle, 9:6, 1167-1181, DOI: 10.4161/cc.9.6.11067

To link to this article: https://doi.org/10.4161/cc.9.6.11067

Published online: 15 Mar 2010.

Cell Cycle 9:6, 1167-1181; March 15, 2010; © 2010 Landes Bioscience

Differential binding of p53 and nutlin to MDM2 and MDMX

Computational studies

Thomas Leonard Joseph,[1,†] Arumugam Madhumalar,[1,†] Christopher John Brown,[2] David P. Lane[2] and Chandra Verma[1,*]

[1]Bioinformatics Institute (A-STAR); Matrix, Singapore; [2]p53Lab (A-STAR); Immunos, Singapore

[†]These authors contributed equally to this work.

Key words: p53, MDM2, MDMX, nutlin, molecular simulations

Half of human tumours have mutated p53 while in the other half, defective signalling pathways block its function. One such defect is the overexpression of the MDM2 and MDMX proteins. This has led to an intense effort to develop inhibitors of p53-MDM2/MDMX interactions. Nutlin is the first such compound described to block p53-MDM2 interactions. Molecular dynamics simulations have been used to explore the differences in binding of p53 and nutlin to MDM2/MDMX. Simulations reveal that p53 has a higher affinity for MDM2 than MDMX, driven by stronger electrostatic interactions. p53 is displaced from MDM2 by nutlin because it is more flexible, thus paying a larger entropic penalty upon sequestration by MDM2. The inherent plasticity of MDM2 is higher than that of MDMX, enabling it to bind both p53 and nutlin. The less flexible MDMX interacts with the more mobile p53 because the peptide can adapt conformationally to dock into MDMX, albeit with a reduced affinity; nutlin, however is rigid and hence can only interact with MDMX with low affinity. Evolutionarily, the higher affinity of MDM2 for p53 may enable MDM2 to bind p53 for longer periods as it shuttles it out of the nucleus; in contrast, MDMX only needs to mask the p53 TA domain. This study enables us to hypothesize gain of function mutations or those that have decreased affinity for nutlin. These conclusions provide insight into future drug design for dual inhibitors of MDM2 and MDMX, both of which are oncoproteins found overexpressed in many cancers.

Introduction

The tumour suppressor protein p53, also called "the guardian of the genome",[1] plays a key role in maintaining the integrity of eukaryotic cells. Upon cellular stress, p53 is stabilized and activates pathways that can either lead to cell cycle arrest, senescence or apoptosis.[2,3] The levels of p53 in normal cells are tightly maintained by the *Murine Double Minute 2* (MDM2) oncoprotein in an important negative feed back loop. MDM2, whose transcription is stimulated by p53, prevents transactivation of other target genes by p53 as well as targeting it for degradation.[4] MDM2 interacts with p53, via the N-terminal transactivation (TA)[4] and the DNA-binding (DBD) domains of p53,[5] and then stimulates ubiquitination of p53 followed by its proteosomal degradation. More recently MDM2 has also been shown to associate with the mRNA of p53 and regulate p53 translation.[6,7] When normal cells undergo stress, posttranslational modifications induce the release of p53 from its negative regulator, MDM2. This is primarily achieved through the phosphorylation of the N-terminus of both the proteins, which disrupts the MDM2-p53 interaction, leading to the accumulation of p53.[3] Indeed, many cancer cells have overexpressed MDM2, leading to the degradation of p53.[8-11]

MDMX (also known as MDM4), a close homolog of MDM2, is another negative regulator of p53.[12,13] MDMX potentiates the ubiquitin ligase activity of MDM2 and enhances p53 degradation.[14-16] Both MDM2 and MDMX regulate p53 through interactions mediated by their N-terminal domains and the N-terminal TA domain of p53. However, unlike MDM2, MDMX is not a functional ubiquitin E3 ligase or a target for p53 transactivation.[14-16] The residues Phe19, Trp23 and Leu26, located in the TA domain of p53, contribute a majority of the binding energy in the interaction of p53 with both MDM2 and MDMX.[17-21] MDM2 also ubiquitinates MDMX and targets it for proteosomal degradation.[22] MDMX has also been found to be overexpressed in several cancers.[23] Elevated MdmX mRNA occurs in tumours with wild-type p53, and MdmX knockdown in breast carcinoma and retinoblastoma cell lines leads to p53-dependent growth-arrest or apoptosis.[24-26] This implies that in the absence of any other regulatory changes, MdmX-dependent inhibition of p53 is also critical for tumorigenesis. The inhibition of the p53 interaction with MDM2 and MDMX has been shown to be therapeutically important[27] and hence it is essential to develop a detailed understanding of the structural and energetic aspects of these interactions.

*Correspondence to: Chandra Verma; Email: chandra@bii.a-star.edu.sg
Submitted: 11/19/09; Revised: 12/22/09; Accepted: 12/28/09
Previously published online: www.landesbioscience.com/journals/cc/article/11067

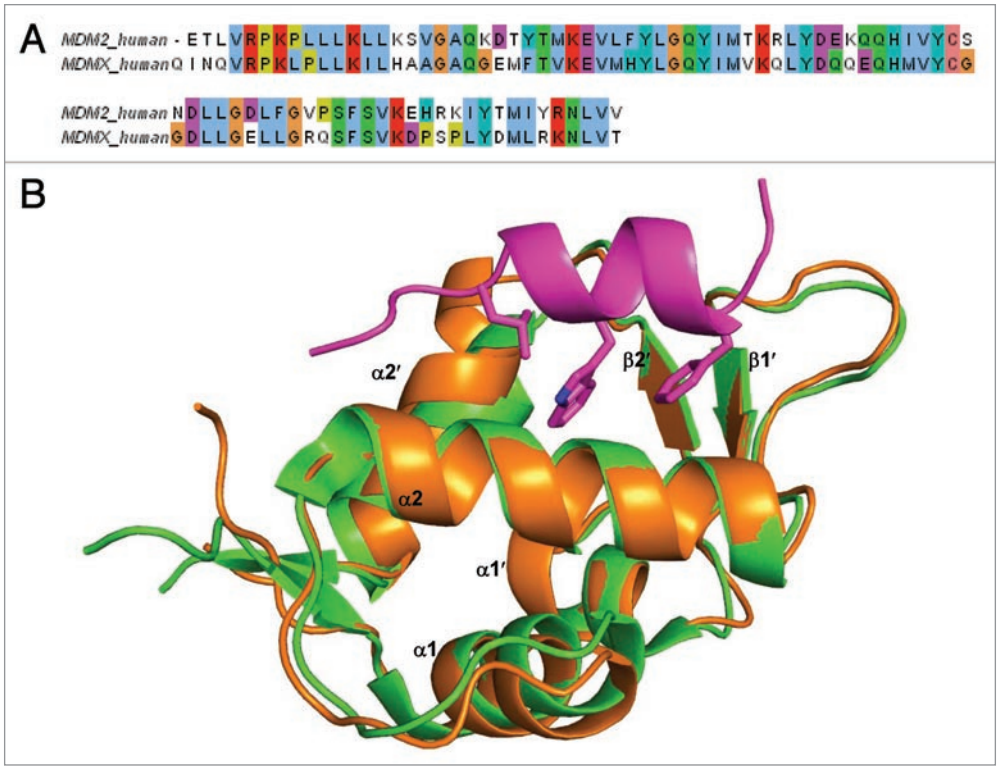

Figure 1. (A) Sequence alignment of MDM2 (25–109) and MDMX (23–108); (B) The crystal structures of p53 complexed to MDM2 (orange, 1YCR.pdb) and MDMX (green, 3DAB.pdb) shown superposed with the three key interacting residues of p53 shown in sticks. For clarity only the p35 peptide (in magenta) from 1YCR is shown.

The N-terminal domains of MDM2 and MDMX are similar in sequence (identity ~54%, **Fig. 1A**) and their crystal structures in complex with a p53 TA domain derived peptide (hereafter referred to as the p53 peptide) have been determined, revealing the same overall structural fold and similar interactions (**Fig. 1B**). The p53 bound states of both MDM2 and MDMX show that the environments are highly similar for Phe19 and Trp23 but not for Leu26. The key differences lie at 3 positions—Leu54 in MDM2, Met53 in MDMX; His96 in MDM2, Pro95 in MDMX and Ile99 in MDM2, Leu98 in MDMX (**Fig. 2A and B**). Several peptides, small molecules and peptidomimetics have been identified as inhibitors of this interaction between p53 and MDM2/MDMX.[17,24,28-37] The crystal structure of nutlin complexed to MDM2, PDB code 1RV1,[28] has been resolved at 2.3 Å. It shows (**Fig. 3A**) that the chemical groups of nutlin (**Fig. 3B**) mimic the three key interactions of p53 mentioned above: the imidazoline sits on the binding site projecting three hydrophobic groups into subpockets that are occupied by the Phe19, Trp23 and Leu26 side chains in MDM2, while the piperazine ring (as a solubilising group) attached to the N1 of the imidazoline remains outside the binding site and does not contact MDM2. However nutlin is dramatically weaker in its ability to disrupt the interaction between MDMX and p53.[24,25,38] Recently several high affinity phage derived peptides have shown vast improvements in their dual affinity for both MDM2 and MDMX.[22,24,32,34,36]

While much insight has been gained in structural biology and drug discovery using experimental techniques such as NMR and crystallography, it is increasingly becoming clear that the underlying dynamics[39,40] are critical. Towards this goal, the technique of molecular dynamics (MD) simulations have been applied extensively to investigate biochemical phenomena.[41,42] Several groups have applied MD to understand the binding of p53 peptides to MDM2,[18-20,32,43-47] and MDMX[48-50] providing valuable insights into this interaction. Here we examine the differential binding of p53 peptide and nutlin to MDM2 and MDMX using MD simulations. This, to our knowledge, has not been reported elsewhere. We then turn our attention towards asking if our methods could usefully be employed in gaining some understanding of the development of resistance in tumours to both nutlin treatment and for gain of function in MDM2. The development of resistance to drugs and gain of function mutants of p53, MDM2 is of much clinical interest.[51-53]

Results

The MD simulations were judged to be stable as evidenced by the time dependant evolution of RMSD and radius of gyration (**Fig. S1A–D**). The positional fluctuations of the Cα atoms (**Fig. 4A–C**) show that MDMX is more mobile than MDM2 in its apo as well as in its complexed states. This mobility is particularly pronounced in the loops that connect α2 and β1', β1' and α1', β2' and α2' (**Fig. 1B**). These are also the regions that display differential fluctuations between the two proteins. Residues Glu69, Lys70 and Val93 have the largest fluctuations in MDM2

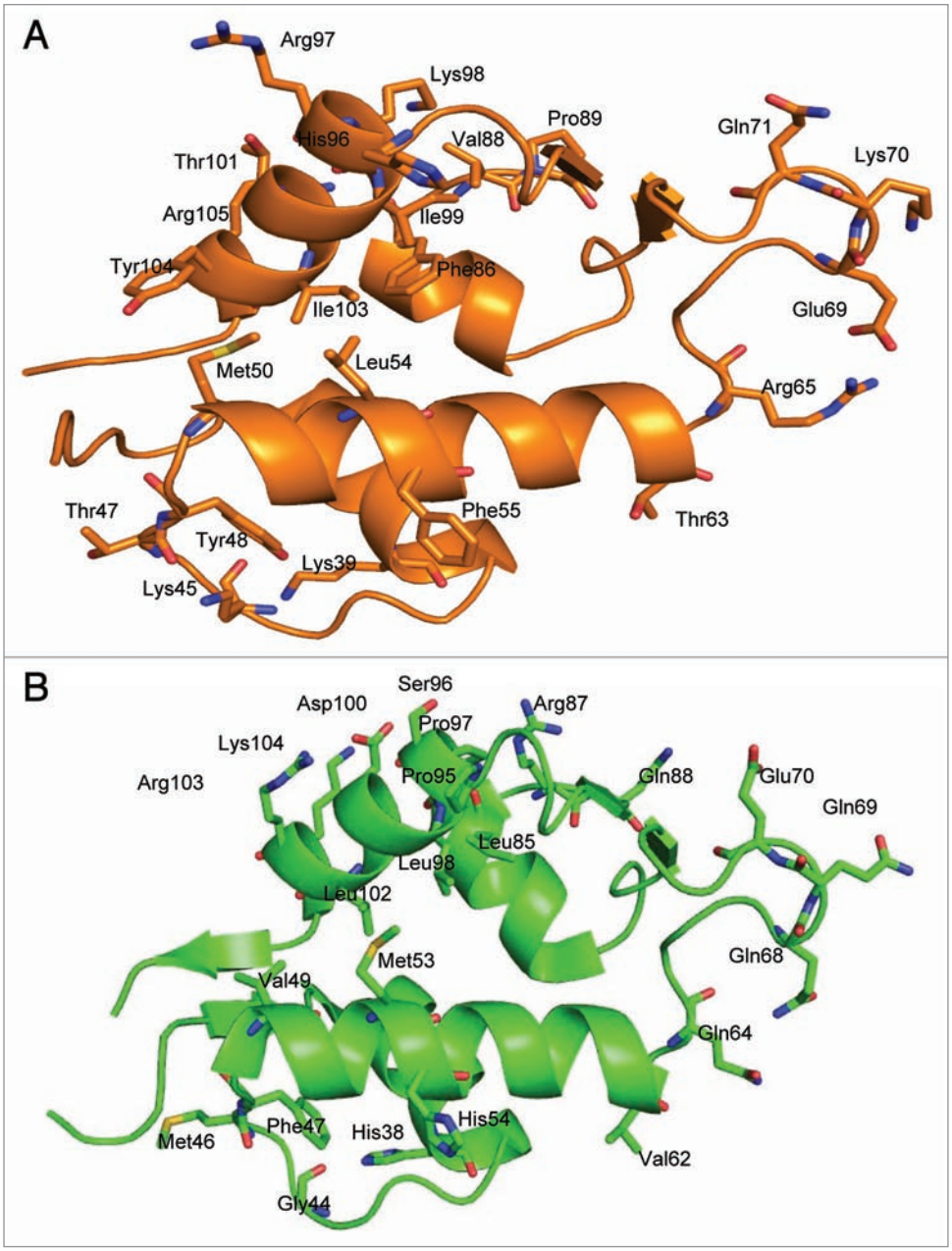

Figure 2. The differences in residue location and composition of MDM2 (orange, A) and MDMX (green, B).

while Gln69, Glu70, Asp79 and Asp94 have the largest fluctuations in MDMX. These residues are also in the neighbourhood of the ligand/peptide binding sites of both proteins (**Fig. 2A and B**). The largest differences in fluctuations are seen in the β2'-α2' loop and are two-fold larger in MDMX. We probe the origin of this in later sections. Overall, the region encompassing the β2'-α2' loop and the α2' helix displays higher flexibility in both MDM2 and in MDMX in their apo and nutlin-bound states than in their p53 bound states. This region interacts with p53 but not with nutlin, thus leading to the observed higher mobility in the presence of nutlin. The peptides, when bound, show a large difference at the Cterminus, with much larger mobility in MDMX (**Fig. 4D**).

Protein motions of MDM2 and MDMX in the free and complexed states. The nature of motions explored by MDM2/MDMX during the simulations can best be assessed by computing their phase space portraits. The technique of principal component analysis (PCA) is the most widely used for this purpose.[54-57] This technique decomposes the intrinsic flexibility of a protein into motions of different frequencies of vibrations. These are then ordered such that the first component (PC1) characterizes the motion with the largest amplitude and lowest frequency. The advantage of this technique is that it enables a direct comparison with experimentally determined structural data. Principal components were computed for MDM2 and MDMX in their various states: apo, complex with p53 and complex with nutlin. From

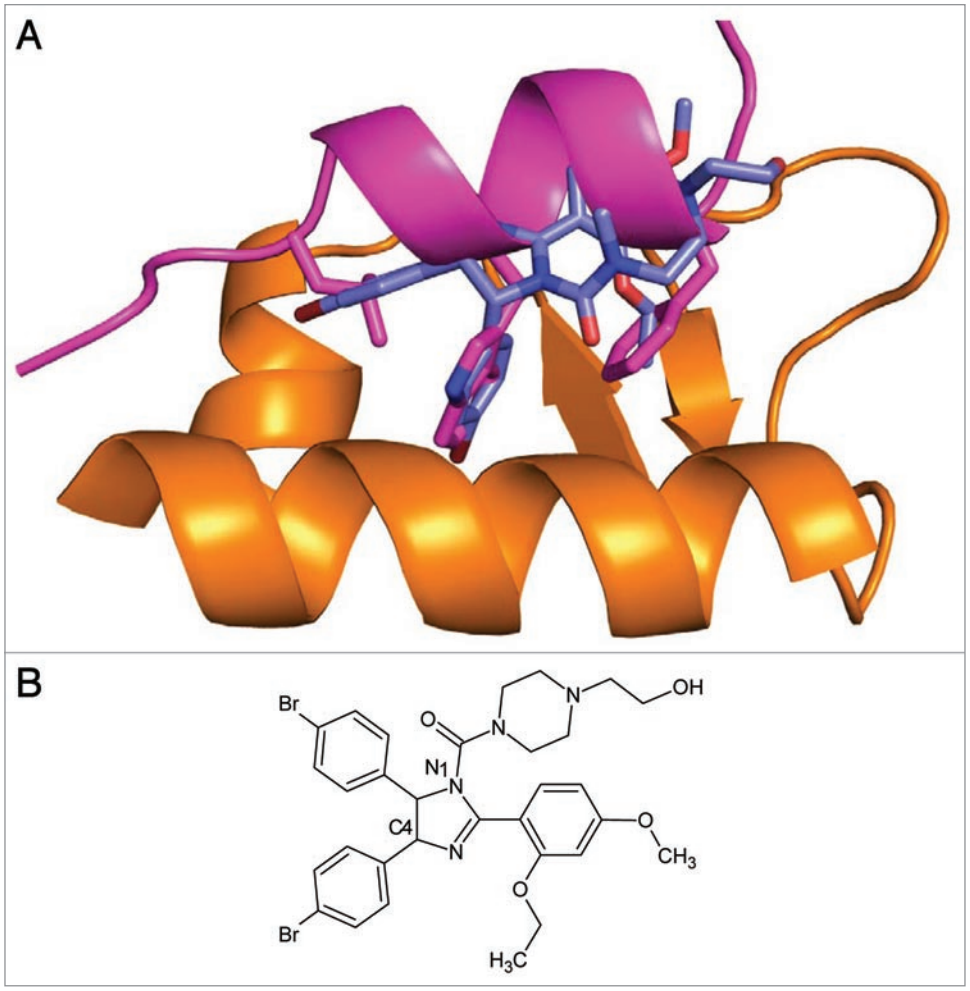

Figure 3. (A) Nutlin2 (blue sticks) complexed to the p53-binding pocket of MDM2 (orange) taken from the crystal structure 1RV1 and superposed on to the structure of p53 peptide when complexed (magenta, taken from 1YCR.pdb). (B) The chemical structure of nutlin2.

Figure 5A and B it is clear that PC1 (Principal Component 1) dominates the motions of MDM2 (covering 30–37% of overall motion). In contrast, the motion is more distributed across other modes in MDMX (**Fig. 5A and B** inset). The extent of the coverage of phase space or entropy in MDM2 is in the order apo > nutlin > p53. This is understandable since p53 makes extensive contacts with MDM2 than does nutlin, and hence is much less flexible. When we examine the distributions in this space of the experimentally determined structures of MDM2, we find that the phase space of apo simulations covers the structures of apo MDM2 determined by NMR; indeed the simulations cover a larger region of phase space. Comparing the data for the complexes, we find that the MDM2 crystal structures divide into two regions of the phase space: the ones that are closer to the p53-MDM2 complex simulations are those representing MDM2 crystal structures complexed to peptides or peptidomimetics. In contrast, the structures that are within the region of phase space covered by the MDM2-nutlin simulations are those crystals where MDM2 is complexed to small molecules. Together, this suggests that our simulations are indeed covering regions of phase space that truly represent the experimental states. Indeed, the fact that our apo simulations cover the experimental data, despite the fact that our apo state was derived from the complex of MDM2 with p53, further strengthens the validity of our simulations. In MDMX, the coverage of phase space by the apo protein is much smaller than for MDM2, highlighting its lower flexibility (and hence adaptability). When complexed to p53 and to nutlin, the coverage is somewhat larger than in MDM2; it is more pronounced for nutlin. As we shall see later, this rationalizes the basis of differential binding. The experimental states of MDMX are covered by the simulations; there is no small molecule-MDMX structure available.

Evolution of the secondary structures during the simulations show that in its free state, the p53 peptide (**Fig. S2**) can exist as interconverting conformers, with the helical conformation dominant, in particular in the region Phe19-Trp23 (the region essential for binding to MDM2/MDMX). This is in agreement with experimental (NMR observations show that the Thr18-Leu26 region is helical in solution[58]) and with other simulation studies.[18,19,59] Interestingly, the p53 peptide exists as a somewhat longer helix when complexed with MDM2 (**Fig. S2**) than with MDMX. This difference arises because during the MD simulations, the

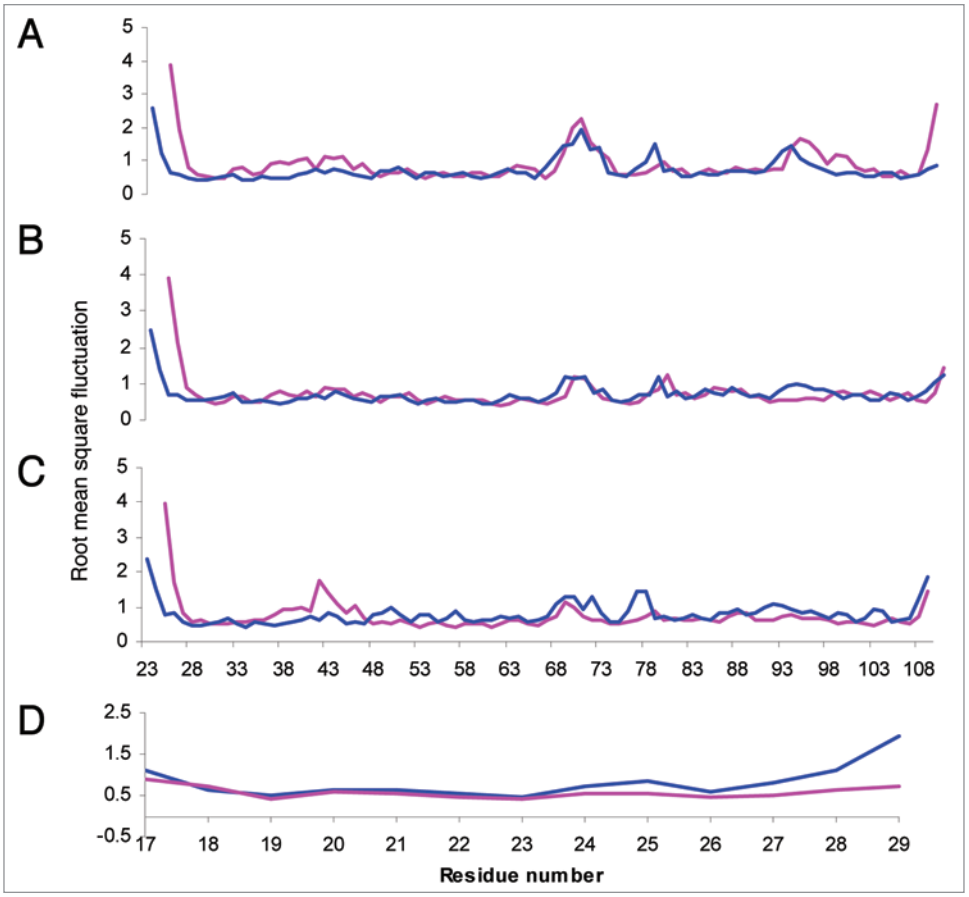

Figure 4. Root mean squared fluctuations of the Cα atoms of MDM2 (in magenta) and MDMX (in blue) in their (A) apo (B) p53-complexed (C) nutlin-complexed states. (D) Root mean squared fluctuations of Cα atoms of p53 when complexed to MDM2 (magenta) and MDMX (blue).

anionic Glu17 of p53 forms a salt bridge with Arg65 in MDM2 (**Fig. 2A**) resulting in the p53 adopting an extra helical turn at its N-terminus (this is not possible in MDMX since the equivalent residue is Gln64, **Fig. 2B**).

Hydrogen bond patterns in the complexed states of MDM2 and MDMX. We next investigated the hydrogen bond (hbond) landscapes of the two complexes. The crystal structure 1YCR shows the following hbonds between p53 and MDM2: Glu17 and MDM2-Lys94 side chains, Asp21 side chain and Thr18 backbone, Trp23 side chain and MDM2-Leu54 backbone, Asn29 and MDM2-Glu25 side chains and between the C-terminal carboxylate of p53 and MDM2-Tyr100/Tyr104 side chains (**Fig. S3A**). During the simulations of the p53-MDM2 complex the only hbond that is retained is that between Trp23-Nε1 and Leu54-CO. The intra peptide Thr18-Asp21 hbond exists for only 8% of the total time; there is an hbond between Glu17-CO and Ser20-Oγ for about 49% of the simulation, which arises from the extra helicity of the peptide at the N-terminal. This extra turn is enabled because of a salt bridge that is formed dynamically between Glu17 of p53 and Arg65 of MDM2. In the crystallographic state, Arg65 is 15.7 Å from Glu17 and is hbonded to Glu69 of a neighbouring MDM2 molecule while Glu17 interacts weakly with Lys94. However, during the simulations, with the constraint imposed by the symmetry copies released, localized fluctuations disrupt this weak Glu17-Lys94 interaction. By 3 ns, Glu17 undergoes large fluctuations (characteristic of terminal residues) and moves towards Arg65, which is stabilized also by Tyr67. By 7 ns this Glu17-Arg65 interaction has stabilized and remains stable for the subsequent 8 ns. This Arg65 is replaced by Gln64 in MDMX and hence this salt bridge with Glu17 cannot form.

The crystal structure 3DAB shows the following hbonds between the p53 peptide and MDMX: between Trp23-Nε1 and the Met53-CO, between Phe19-N and Gln17-Oε1 (**Fig. S3B**). In the simulations of the p53-MDMX complex, the former hbond was retained with an occupancy of 48%. The Phe19 and Trp23 backbones make an hbond whose occupancy during the simulation is 66%. In summary, it appears that the additional hbonds in p53 complexed to MDM2 enables it to have a stabler and longer helix than when complexed to MDMX.

The crystal structure 1RV1 also shows an hbond between Gln72-Nε1 and hydroxyl attached to the piperazine moiety of nutlin (**Fig. S3C**). During the simulation this hbond is lost and this group remains exposed to solvent water. The MDMX-nutlin structure was modelled and contains no hbonds between nutlin and MDMX either in the beginning or during the simulations; the hydroxyl attached to the piperazine moiety again remains exposed to solvent, as in the MDM2-nutlin simulation.

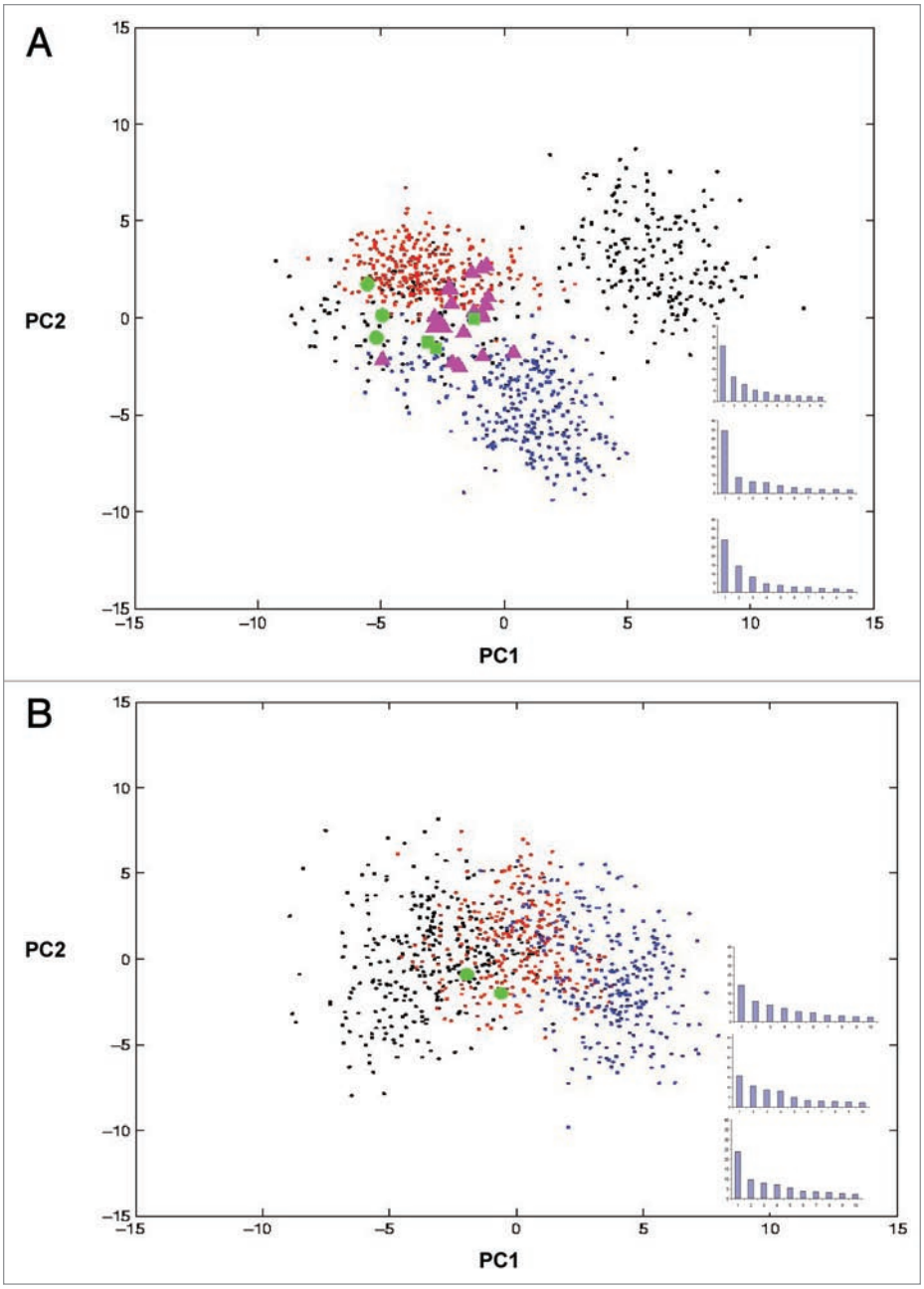

Figure 5. The distribution of the structures in the phase space defined by principal components 1 and 2 showing that the apo states of MDM2 are more flexible than MDMX and capture the variations seen in both simulated and experimental structures. MDM2 covers the region also occupied by p53 bound and nutlin bound states, highlighting its adaptability; in contrast MDMX is much more clustered in all its states. The black, red and blue dots represent the respective simulations in apo, p53-bound and nutlin bound states for MDM2 (A) and MDMX (B). Green circles represent the crystal structures of MDM2/MDMX complexed with peptides; Green squares represent the crystal structures of MDM2 complexed with small molecules; Majenta triangles represent the structures of apo MDM2 derived by NMR. Inset histograms refer to the contributions of individual principal components to the overall fluctuations and, in descending order, refer to the apo, p53-complex and nutlin-complex respectively for MDM2 (in A) and MDMX (in B).

Energy calculations for the MDM2 and MDMX with the p53 peptide and nutlin. *Free energy of binding of p53.* The ΔG_{bind} of p53 and MDM2 was computed to be -6.4 kcal/mol (**Table 1**) which is close to both experimental[60,61] (-6.6 to -7.8 kcal/mol) and other computational estimates[18,20] (-6.9 to -7.4 kcal/mol). In contrast, ΔG_{bind} for p53 and MDMX is computed to be -3.7 kcal/mol (**Table 2**); this trend is in accord with experimental estimates that MDMX has a lower affinity for p53.[17,60,61] With this benchmark established, we now examine the origins of these differences.

Global electrostatics of MDM2 and MDMX (**Fig. S4**) show that MDM2 is highly cationic compared to MDMX with net charges being +5 and +1 respectively. This is seen in a larger intramolecular electrostatic energy component of MDM2 (**Tables 1 and 2**). Indeed dynamic electrostatic maps (**Suppl. movies SM1–SM5**) show that the surface of p53 is complementary to that of highly cationic MDM2 than it is to the MDMX surface. This also suggests that k_{on} of the p53 peptide (net charge -2) for MDM2 may be higher than for MDMX. It is also likely that the weaker interactions of p53 with MDMX (**Tables 1 and 2**) may lead to a higher k_{off}. Together these may partly explain why the affinity of p53 for MDMX is very low compared to that for MDM2.[17] A further clue emerges from inhibition studies of Lane and colleagues[17,61] where the removal of a negative charge from p53, by mutating Glu17, lead to a lower affinity for MDM2, while the change for MDMX was smaller. The free energy of binding of the p53 peptide and MDM2/MDMX is enthalpically driven in both cases; in MDM2, enthalpy dominates entropy by an excess of 15%, while in MDMX, it does so only by 6%. The enthalpic component in MDM2 is 25% stronger than it is in MDMX and clearly originates in the electrostatic interactions (-494.2 vs. -146.1 kcal/mol respectively; **Suppl. movies SM6 and SM7**).

Despite the structural differences we have seen above, the fact that the van der Waals interactions are similar (~-52 kcal/mol) suggests that the packing is driven largely by the interactions of Phe19, Trp23 and Leu26, which are conserved in the two complexes. As expected, the penalty paid for burying charges upon complexation is higher (~3-fold) in MDM2-p53. Entropically, the vibrational contribution in MDM2 is twice as stabilizing as it is in MDMX. This is expected because the amplitude of motion as described by the

Table 1. Components of binding free energy (in kcal/mol) of MDM2 with p53 peptide

	MDM2-p53		MDM2		p53		Delta
	Mean	Std	Mean	Std	Mean	Std	
ELE	-3043.9	78.3	-2378.8	48.9	-170.9	26.8	-494.2
VDW	-395.4	16.6	-319.0	15.2	-23.8	6.2	-52.6
INT	1743.6	28.6	1516.6	26.1	224.3	11.1	2.8
GAS	-1695.7	83.1	-1181.2	53.0	29.6	27.9	-544.1
GBSUR	35.0	0.8	32.9	0.6	10.0	0.4	-7.9
GB	-1296.6	69.6	-1321.2	43.0	-484.0	25.4	508.6
GBSOL	-1261.6	68.9	-1288.3	42.7	-474.0	25.4	500.7
GBELE	-4340.5	17.5	-3700.0	15.0	-654.9	4.7	14.4
GBTOT	-2957.3	30.5	-2469.5	27.6	-444.4	11.3	**-43.4**
TSTRA	16.2	0.0	16.0	0.0	14.4	0.0	-14.3
TSROT	16.0	0.0	15.8	0.0	13.1	0.1	-12.9
TSVIB	1180.7	4.6	1025.7	4.2	164.8	2.8	-9.9
TSTOT	1212.9	4.6	1057.6	4.2	192.3	2.9	**-37.0**
ΔG_{bind}							**-6.4**

Table 2. Components of binding free energy (in kcal/mol) of MDMX with p53 peptide

	MDMX-p53		MDMX		p53		Delta
	Mean	Std	Mean	Std	Mean	Std	
ELE	-2932.7	61.2	-2615.7	46.4	-170.9	26.8	-146.1
VDW	-406.0	14.6	-330.0	14.0	-23.8	6.2	-52.2
INT	1760.6	28.2	1542.0	25.5	224.3	11.1	-5.6
GAS	-1578.1	66.0	-1403.7	52.2	29.6	27.9	-204.0
GBSUR	36.6	0.7	33.4	0.5	10.0	0.4	-6.8
GB	-1377.1	56.0	-1068.8	41.9	-484.0	25.4	175.8
GBSOL	-1340.5	55.6	-1035.5	41.8	-474.0	25.4	169.0
GBELE	-4309.7	16.2	-3684.5	14.6	-654.9	4.7	29.6
GBTOT	-2918.6	29.9	-2439.2	28.2	-444.4	11.3	**-35.0**
TSTRA	16.2	0.0	16.0	0.0	14.4	0.0	-14.3
TSROT	16.1	0.0	15.9	0.0	13.1	0.1	-12.9
TSVIB	1183.1	5.6	1022.4	4.8	164.8	2.8	-4.1
TSTOT	1215.4	5.7	1054.3	4.8	192.3	2.9	**-31.2**
ΔG_{bind}							**-3.7**

lowest frequency mode (as evidenced from principal components of the fluctuations)[62-64] is higher in MDM2 than it is in MDMX (**Fig. 5A and B**).

Free energy of binding of nutlin. Experiments have demonstrated that nutlin displaces p53 from MDM2 and has a low affinity for MDMX;[24,26] our own simulations concur with these (**Tables 3 and 4**). The interaction with MDM2 is enthalpically driven and dominated by van der Waals interactions which arise mainly from the differential packing of the residues near the binding pocket (mainly from the loop connecting β2' and α2' and the residues comprising helix α2' as we have seen above, **Fig. 4C**). Structurally the nutlin interactions with MDMX are not very stable and this is reflected in the reduction of the interaction energy by ~35%. These interactions are destabilized due to MDMX having a smaller binding pocket than MDM2. This arises largely due to the Leu54 in MDM2 replaced by the larger Met53 in MDMX. As a result, the electrostatic and van der Waals components of the interactions are 3-fold and 30% stronger respectively in MDM2 than in MDMX. The relatively small differences in the entropic components arise because nutlin is small and rigid. In contrast, the p53-MDM2 interaction extends over a large interface. This results in a larger vibrational entropy.[19] In the case of the p53-MDMX complex, the p53 does not have the extra helical turn which results in a smaller interface and hence lower vibrational entropy.

Binding of p53 to MDM2 is largely electrostatically driven but does have a significant van der Waals component (arising from extensive packing against a large surface). However, the burial of charged residues upon complexation with p53 is penalized and on balance it turns out that the enthalpic components of the binding of both p53 and of nutlin to MDM2 are similar. In contrast, the reduction of p53 upon sequestration by MDM2 incurs a larger entropic penalty than does nutlin because p53 is larger and more flexible (**Tables 1 and 3**). This leads to a higher affinity of nutlin for MDM2. In contrast, the reduced affinity of nutlin over p53 for MDMX arises from both reduced electrostatic as well as van der Waals components (**Tables 2 and 4**). The relatively more open and less stable binding site of MDMX (in contrast to that of MDM2) is unable to yield a well-packed complex with nutlin.

Energetic contributions of individual residues in the p53 peptide. The contributions of the individual residues of p53 to its binding to MDM2 and MDMX are dominated by the three critical residues of p53 (Phe19, Trp23 and Leu26, **Table 5**), and also by Leu22; this is in accord with experimental[17] and other computational studies.[18,19] The C-terminal of p53 cannot embed in the binding pocket of MDMX due to the bulky Met53 leading to diminished interactions (~kT) of Leu25, Leu26, Pro27, Glu28 and Asn29 (**Table 5**). The residues comprising the helix α2' in MDMX (Pro95/Tyr99) do not pack well against Leu25/Leu26 of p53 in contrast to equivalent residues in MDM2 (His96/Tyr100) (**Fig. 6A and B**). This arises because the local topology in MDM2 creates a curvature that nestles Pro27 (**Fig. 6A**); this feature is missing in the MDMX surface (**Fig. 6B**). This is further associated with a favourable interaction between Asn29 of p53 and Glu25 of MDM2. This is not possible in MDMX as there is no anionic residue in the vicinity (the equivalent residue in MDMX is Q26).

The energetic contributions of the residues to binding of p53 follows the order: Phe19 > Trp23 > Leu26 > Leu22 (Phe19 contributes ~1 kcal/mol more favourably than Trp23; this is due to a higher desolvation penalty for the polar sidechain of Trp23) for both MDM2 and MDMX with almost equal contributions in both proteins. The discrimination of 8 kcal/mol in favour of MDM2 arises from Leu25 (excess of 2 kT), Pro27 (~2.5 kT) and Asn29 (~6 kT).

Among the residues of MDM2 (**Fig. 7A–C**), Arg65, Lys70, Arg97 and Lys98 make large stabilizing electrostatic contributions and do not have equivalent contributions in MDMX; a similarly stabilizing Arg103 in MDMX does not have an equivalent

Table 3. Components of binding free energy (in kcal/mol) of MDM2 with nutlin

	MDM2-nutlin		MDM2		Nutlin		Delta
	Mean	Std	Mean	Std	Mean	Std	
ELE	-2463.3	58.3	-2378.8	48.9	-62.4	3.6	-22.2
VDW	-353.8	15.3	-319.0	15.2	12.3	3.0	-47.1
INT	1616.3	28.4	1516.6	26.1	108.2	6.3	-8.5
GAS	-1200.8	62.0	-1181.2	53.0	58.2	6.9	-77.8
GBSUR	32.9	0.7	32.9	0.6	5.4	0.1	-5.4
GB	-1306.1	50.8	-1321.2	43.0	-24.6	1.9	39.7
GBSOL	-1273.2	50.5	-1288.3	42.7	-19.2	1.8	34.3
GBELE	-3769.4	15.2	-3700.0	15.0	-87.0	2.2	17.5
GBTOT	-2474.0	30.3	-2469.5	27.6	39.0	6.2	**-43.5**
TSTRA	16.1	0.0	16.0	0.0	13.6	0.0	-13.6
TSROT	15.9	0.0	15.8	0.0	11.8	0.0	-11.8
TSVIB	1074.2	6.7	1025.7	4.2	48.7	0.3	-0.3
TSTOT	1106.2	6.7	1057.6	4.2	74.2	0.3	**-25.6**
ΔG_{bind}							**-17.9**

Table 4. Components of binding free energy (in kcal/mol) of MDMX with nutlin

	MDMX-nutlin		MDMX		Nutlin		Delta
	Mean	Std	Mean	Std	Mean	Std	
ELE	-2686.7	39.5	-2615.7	46.4	-62.4	3.6	-8.7
VDW	-352.3	15.4	-330.0	14.0	12.3	3.0	-34.6
INT	1655.9	30.8	1542.0	25.5	108.2	6.3	5.7
GAS	-1383.1	50.4	-1403.7	52.2	58.2	6.9	-37.5
GBSUR	33.9	0.7	33.4	0.5	5.4	0.1	-4.8
GB	-1075.0	34.5	-1068.8	41.9	-24.6	1.9	18.4
GBSOL	-1041.1	34.2	-1035.5	41.8	-19.2	1.8	13.6
GBELE	-3761.7	14.4	-3684.5	14.6	-87.0	2.2	9.7
GBTOT	-2424.2	31.1	-2439.2	28.2	39.0	6.2	**-24.0**
TSTRA	16.1	0.0	16.0	0.0	13.6	0.0	-13.6
TSROT	15.9	0.0	15.9	0.0	11.8	0.0	-11.8
TSVIB	1072.7	5.2	1022.4	4.8	48.7	0.3	1.6
TSTOT	1104.7	5.2	1054.3	4.8	74.2	0.3	**-23.7**
ΔG_{bind}							**-0.3**

contribution in MDM2. It is interesting that of these residues, none make direct interactions with p53 in the crystal structure, thus further emphasizing the importance of understanding the dynamics of these interactions. The destabilizing contributions in both proteins arise from anionic residues and these are conserved across all species (**Fig. 11**). When we examine the van der Waals interactions, we find that the dominant interactions that favour the affinity of p53 for MDM2 are Met62, His96 and Tyr100. The binding of nutlin to MDM2 and MDMX is dominated by packing interactions (**Tables 3 and 4**). The stronger binding of nutlin to MDM2, compared to MDMX, arises predominantly from (energy values in parentheses are in kcal/mol and refer to contributions from MDM2/MDMX): Leu54 (-2.1/-1.4), Gly58 (-1.8/-1.3), Met62 (-1.8/-0.8), Gln72 (-2.3/-1.3) and His73 (-1.4/-0.9) and Val93 (-2.9/-2.4).

Discussion

We have carried out MD simulations of MDM2 and MDMX in three states—apo, complexes with p53 peptide and with nutlin. The phase space covered during the simulations encapsulates the experimentally determined structures of MDM2 and MDMX. This strengthens the reliability of the simulations in reflecting, at the very least, in-vitro conditions. An argument could be made that the simulations were initiated from the crystal structures and hence it is no surprise that they are in the vicinity of such structures; however, these simulations also adequately reflect the motions of the apo states and these structures were determined using NMR, a technique that is very different from crystallography.

How do p53 and nutlin differentiate between MDM2 and MDMX? *Structural basis for differential nutlin binding.* At the N-terminus of the p53 peptide, near the Phe19 pocket, the residues comprising the α2-β1' loop enable better packing of p53 in MDM2 than in MDMX. This enhancement in packing arises due to the favorable interaction of Arg65 with Glu17 of p53; this is not possible in MDMX as the equivalent residue is Gln64. Additional cationicity in this region of MDM2 is brought about by the presence of Lys70. Although this residue does not make direct contacts with Glu17, yet modulates its dynamics through charge-charge interactions; this is replaced by neutral Gln69 in MDMX. Further, in MDM2, Arg65 also interacts with Glu69 of the α2-β1' loop, stabilizing the loop. This in turn provides a compact fit for p53 in MDM2. In MDMX, the corresponding interaction is weakened because the equivalent residue is Gln68.

The Trp23 pocket is similar in both MDM2 and MDMX. In the Leu26 pocket, His96 in MDM2 together with Leu54 and Tyr100 lead to the creation of a cavity that enables a compact fit for Leu25 and Leu26 of p53 (**Fig. 6A and Suppl. movies SM6 and SM7**). In MDMX, this site is occupied by Pro95 which prevents the formation of any such pocket and hence there is no compact fit for Leu26 (**Fig. 6B**). In addition, bulkier Met53 in MDMX localizes in the position occupied by Leu54 in MDM2 (**Fig. 7**). This prevents the Leu26 part of p53 from embedding in MDMX as deep as it does in MDM2. Hence the individual energy contributions from the residues around the Leu26 pocket in MDMX are reduced considerably. In addition, formation of a salt-bridge between Glu95 and Lys98 (70% lifetime) in MDM2, both located in helix α2', further stabilize the Leu pocket. In contrast, in MDMX, this Glu is replaced by Asp94; the shorter side chain of this Asp cannot form a salt bridge since the equivalent residue in MDMX is Pro97. This Asp instead hbonds with Ser96 and also appears to be pulled by long range electrostatic interactions with Arg87 (present in the α1'-β2'), thus pulling this loop (β2'-α2') away from the p53 peptide (this is also evident in the somewhat higher fluctuations, **Fig. 4B**). In the crystal structure, Arg87 makes a salt bridge with Asp94 of a neighboring molecule in the unit cell while Asp94 makes a salt bridge with Arg87 and an hbond with Ser89 of the neighboring subunit of the unit cell through a water molecule. During the simulation,

Table 5. Residue wise energy contributions (in kcal/mol) of the p53 peptide for its interactions with MDM2 and MDMX

	MDM2-p53 complex	MDMX-p53 complex
E17	-0.3	0.2
T18	-0.8	-0.8
F19	-6.6	-6.5
S20	0.0	0.4
D21	0.3	0.3
L22	-2.5	-2.4
W23	-5.5	-5.4
K24	0.6	0.6
L25	-1.7	-0.4
L26	-3.9	-3.4
P27	-2.2	-0.8
E28	0.0	0.1
N29	-1.7	1.2

these neighboring copies do not exist. In addition, the helix α2' in MDMX is destabilized towards the β2'-α2' loop by the presence of Pro95 and Pro97.[27] This salt bridge in MDMX occurs over regions that are spatially separated (α2' and α1'), in contrast to originating in the same secondary structural element in MDM2, appears to facilitate the opening of the Leu26 pocket in MDMX and making it shallow. This further destabilizes the local p53 interactions, which is in accord with experimental observations of Holak and colleagues[50] that the α2' region in MDMX is responsible for the change in the shape of the p53 binding pocket, particularly near the Leu26 binding area. Carotti et al.[48] have also made similar observations from their simulation studies of the MDMX-p53 interactions. We have now isolated the specific interactions that contribute to this local instability. Overall, the α2' region/C-terminal in MDM2 is more positively charged (+3) than it is in MDMX (+1). This presumably enhances the overall affinity of the anionic carboxy terminal of p53. There is a further stabilization of p53 in MDM2 that is brought about by the interaction of Arg97 with the carbonyl backbone of Asn29 and with the anionic carboxy terminal of p53; the equivalent residue in MDMX is Ser96 whose sidechain is not long enough to enable such an interaction. This results in higher mobility of p53 at its C-terminus when complexed to MDMX (**Fig. 4D**).

The bulky side chain of Met53 in MDMX (Leu54 in MDM2) 'pushes' the C-terminal part of p53 against Leu98 and Leu101, effectively occluding this region from p53 (**Fig. 8**). This in turn enables Tyr99 to move to a "closed" conformation (both open and closed conformations have been reported experimentally and computationally);[65] in contrast, the analogous Leu54 in MDM2 is well packed against p53 which remains stably bound, and, Tyr100 is in the "out" position. In summary, it appears that an overall perturbation of the MDMX active site, a concomitant "pushing" out of the p53 peptide, the lack of an extra-helical turn of p53, and, reduced overall intermolecular electrostatic interactions are the source of the lower affinity of p53 for MDMX,[27] (**Figs. 6A and B, 9A and B; Movies SM6, SM7**).

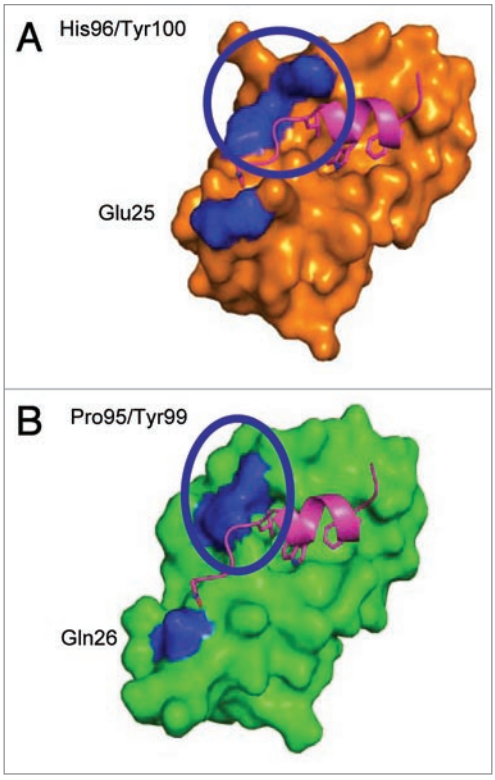

Figure 6. The role of His96/Tyr100 (blue patch) in MDM2 enables the formation of a curvature that embeds the Pro27 of p53 (A). The homologus region in MDMX (Pro95/Tyr99 blue patch) is unable to do so (B). Further stabilization of p53 in MDM2 comes from interactions between the C-terminal region of p53 with Glu25 in MDM2 (A) which is not possible in MDMX (Gln26 in B).

Nutlin reduces the motions observed in MDM2 but not in MDMX. Overall, the pocket of MDMX is more open at the side which docks the N-terminus of p53 and narrow at the side which docks the C-terminus of p53,[27,30,36,66] compared to MDM2 (as seen in the last section); the β2'-α2' loop undergoes much higher fluctuations in the presence of nutlin than in the presence of p53 (**Fig. 4C**). Met53 in MDMX (Leu54 in MDM2) together with Tyr99 make a narrower binding pocket. Pro95 in MDMX, unlike its equivalent His96 in MDM2, cannot reorient and hence makes this region less dynamic (**Fig. 6A and B**). Additionally, in MDM2, correlated motions between Tyr100 and Tyr104 are modulated by interactions with Arg97 and with the N-terminal region of MDM2, which further enables a compaction of the binding site. These dynamic modulations of the binding site are absent in MDMX (**Fig. S5**) where the equivalent residues are Ser96 and Arg103 respectively. This effect is further coupled to the Phe pocket where it is clear that nutlin is embedded deeper in MDM2 than in MDMX. The spatially contiguous α2-β1' loop in MDM2 has Glu69 lying between Lys70 and Arg65 which is replaced in MDMX by polar residues Gln68, Gln69 and Gln64 respectively (**Fig. 2A and B**); the reduced packing and hence higher mobility of the latter is evident in **Figure 4C**. It is clear that these differences are more pronounced for nutlin because it is a small molecule whose binding is driven by short

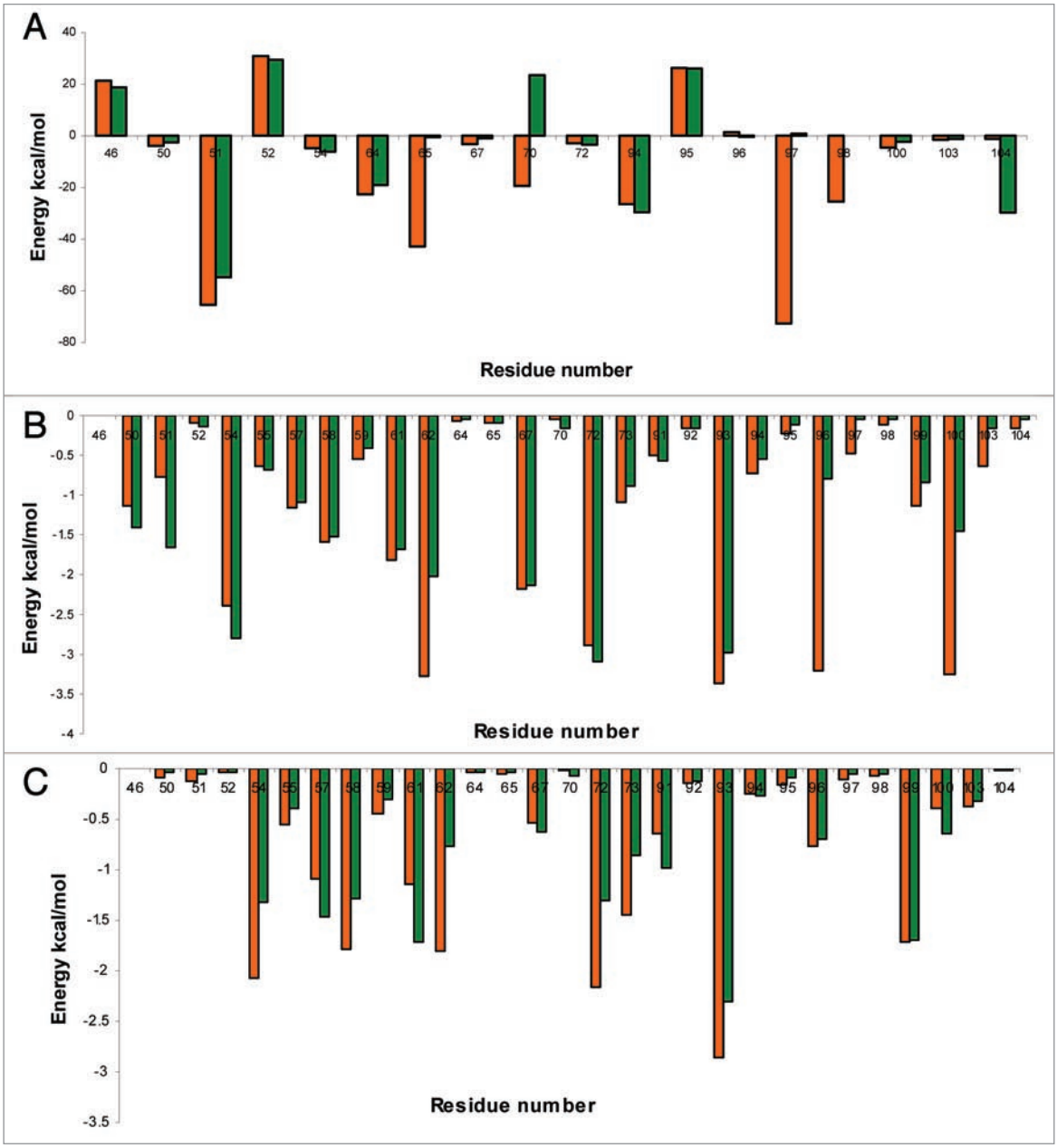

Figure 7. Histogram of contributions of energies by individual residues to the net binding energy of p53 and nutlin to MDM2 (orange) and MDMX (green). (A and B) refer to the electrostatic and van der Waals energies of interactions with p53 respectively; (C) shows the van der Waals interactions with nutlin.

range van der Waals interactions and lacks the long range electrostatics that mediate interactions with p53. For example, the positive charge on Lys51 lies in an anionic field created together by the C-terminus of p53 (**Fig. 10**); this interaction creates a stable binding pocket. Nutlin cannot create this anionic field to constrain Lys51 and hence cannot enable the formation of an analogous pocket. These differences support our earlier findings of how the MDM2 surface (and now MDMX) modulates and is modulated by ligands.[19] Indeed, if we examine the distribution of energies that are associated with the conformational states of the proteins, we see that nutlin does destabilize MDMX by about 11 kcal/mol; **Table ST1** shows that this destabilization originates in the internal strain of MDMX.

These observations suggest the possibility of designing molecules that could modulate the flexibility of MDMX and impart less rigidity to it. This would be analogous to the development of the new class of HIV-integrase drugs where additional pockets were found to be created in the presence of bound molecules.[40]

Biological implications. The above data enables us to hypothesize that the binding site of both MDM2 and MDMX and the associated interactions with p53 have evolved functionally in the following manner: MDM2 needs to hold on tightly to

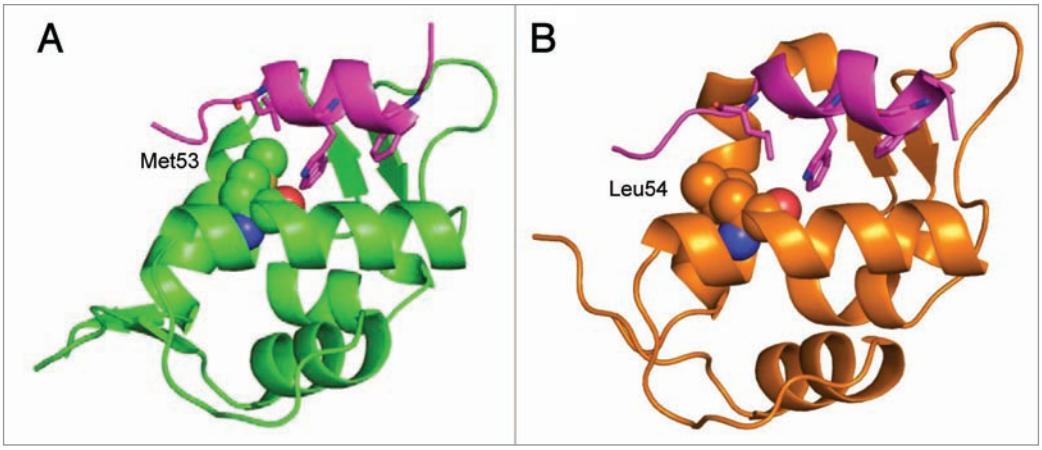

Figure 8. The steric occlusion of p53 due to Met53 in MDMX (A) that does not occur in MDM2 as the equivalent residue is Leu54 (B).

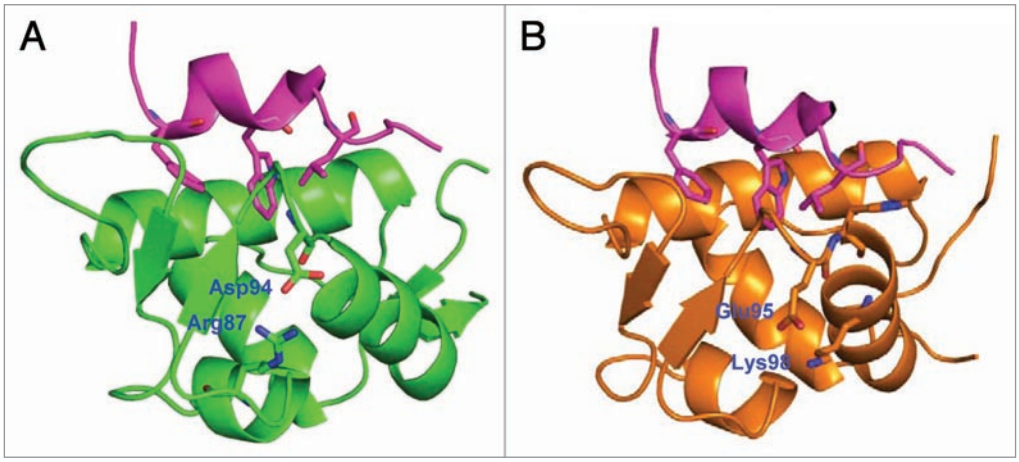

Figure 9. The role of salt bridges in modulating the binding site of p53 in MDM2/MDMX. The Asp94-Arg87 salt bridge in MDMX (A) occurs across different secondary structural elements and opens up the p53-binding pocket in MDMX leading to weaker interactions. In contrast the Glu95-Lys98 salt bridge in MDM2 (B) occurs in the same secondary structural element and thus does not perturb the p53-MDM2 interaction.

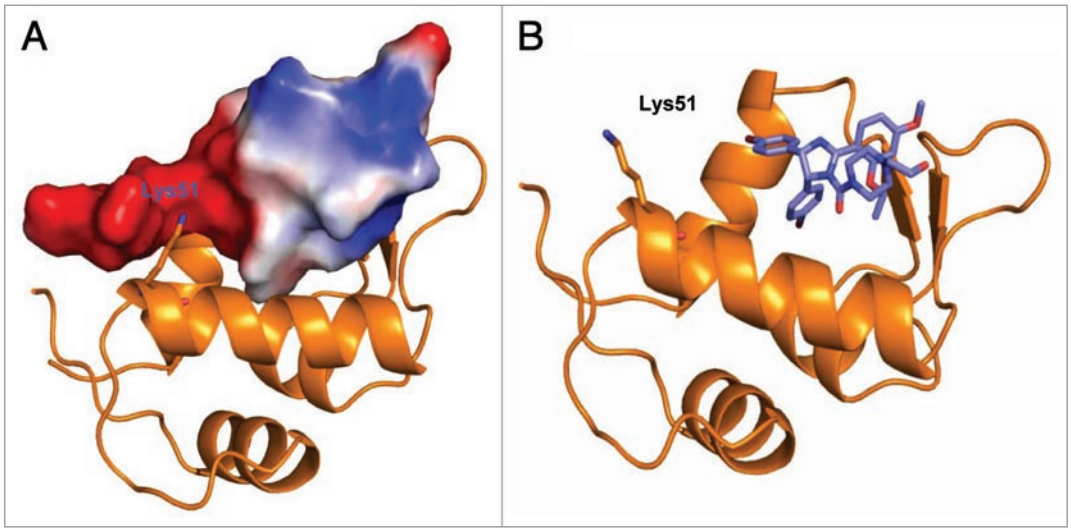

Figure 10. Lys51 stabilizes the interactions with p53 by binding to an anionic potential created by the backbone of p53 in both MDM2 and MDMX (only the structure of MDM2 is shown in A). This interaction is absent in the nutlin complexes (B).

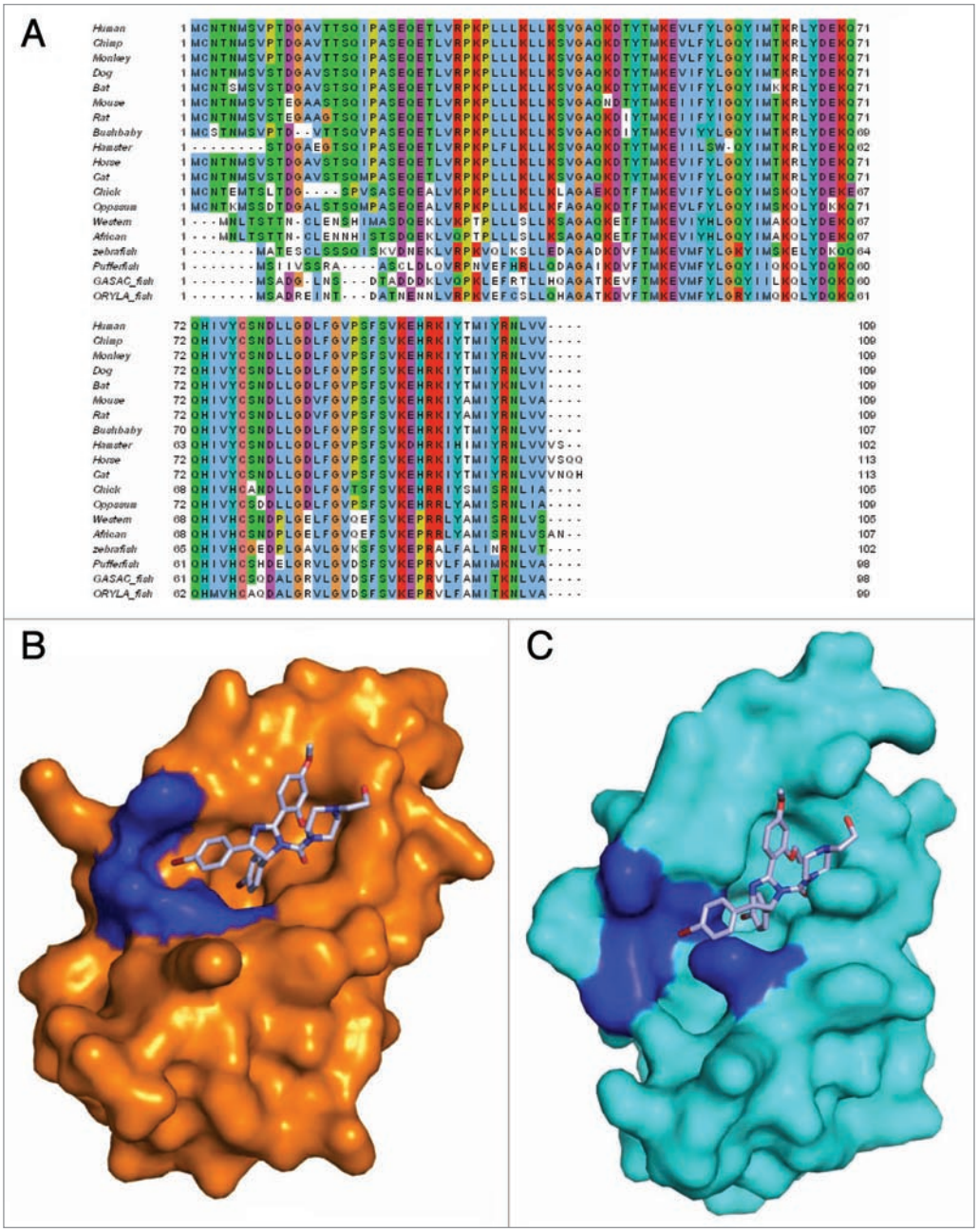

Figure 11. (A) Sequence alignment of the Nterminal domain of MDM2 from different species. (B) Nutlin bound to human MDM2 from the crystal structure 1RV1. (C) Nutlin bound to a homology model of Zebra fish MDM2 constructed using 1YCR. The blue patches show how the cleft in Zebrafish MDM2 (analogous to human MDMX) is narrow and will destabilize the interactions.

p53 as it shuttles it from the nucleus to the cytoplasm. In contrast, MDMX only needs to mask the TA domain of p53 and hence does not need to hold it very tightly. This is also seen in the different flexibilities of the proteins in the PCA plots of the apo proteins, where a larger exploration of phase space by MDM2 reflects its higher intrinsic flexibility. Upon complexation, MDM2 adapts to p53 and binds tightly compared to MDMX and hence the phase space of the MDM2-p53 complex is smaller than that of the MDMX-p53 complex. This will presumably be reflected in very different kinetics of the interaction between MDM2/MDMX and p53 (experimental data on the p53-MDMX is currently lacking). Interestingly we find that the features of MDMX that are largely responsible for occlusion of nutlin are preserved among the MDM2 of lower vertebrates such as fishes (**Fig. 11A**). Indeed, prompted by unpublished data from our lab, which shows that zebrafish MDM2 does not respond to nutlin treatment, we built structural models that clearly point towards a narrowing of the binding cleft, similar to that seen in MDMX (**Fig. 11B and C**).

Oncogenic mutations in MDM2 that can drive cancer development. Having obtained some insights into the key differences that characterize the differential binding of nutlin and

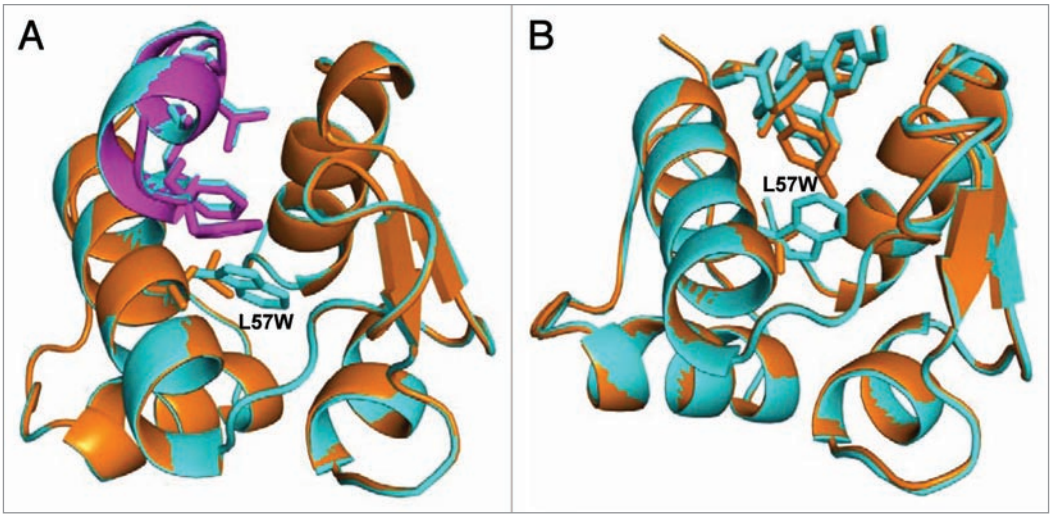

Figure 12. Influence of the hypothetical L57W mutant (wild type MDM2 in orange and mutant MDM2 in cyan) is resistant strain of MDM2 on the binding of p53 (A) and nutlin (B); p35 is shown in magenta in wild type and in cyan in mutant. It is clear that Trp23 of p53 can stack against the mutant sidechain Trp57 and retain binding while nutlin is pushed out of the binding pocket.

the p53 peptide to MDM2/MDMX, we may now ask: is this data sufficient to enable us to hypothesize about the nature of mutations that could arise in MDM2/MDMX in tumours. There have been several insights into developing drugs to bypass resistant mutations. One example was the ingenious design of the so-called "adaptive" inhibitors of the HIV-1 protease. New inhibitors were designed with an intrinsic flexibility that enabled them to adapt structurally to the known resistance mutations in HIV-protease by Friere and colleagues.[67] More recently, a very nice computational study has been used to address resistance mutations and their structural and energetic coupling to inhibitors in EGFR kinase.[68] However it would be nice if a method could be developed that would predict the emergence of mutations at key sites in proteins. Towards this, we begin by asking a simple question: what mutation would enable MDM2/MDMX to destabilize interactions with nutlin and strengthen them with p53, and, what mutations would impart a gain-of-function phenotype to MDM2, i.e., enable it to bind p53 much tighter than does wild type MDM2?

There is very little data available on mutations in the N-terminal domain of MDM2 apart from the work by Levine and colleagues.[69] To rapidly test our hypothesis regarding the emergence of mutations, we first carry out single point calculations, whereby the orientation of the mutated sidechain is energetically optimised using SCWRL,[70,71] and the effects of this on the structure and interactions with p53 and nutlin are computed. For speed, we do not carry out long MD simulations, although a more comprehensive model will certainly have to; we are currently carrying out these studies. We find that the G58D mutation in MDM2 that was found to have abrogated p53 binding by the Levine group, does indeed have a reduced affinity for p53 by 5 kcal/mol (data not shown) relative to the wild type MDM2; as expected the introduction of a negative charge in MDM2 leads to a 20% destabilization of electrostatics. The G58D mutant is located at the periphery of the pocket where Trp23 of p53 embeds and the large change is in accord with the introduction of a charged and bulkier residue (D58). This motivated us to apply the same technique to mutations at sites that were determined based on their interaction energies with p53 and with nutlin in our simulations. For the current study, we chose only a subset of residues of MDM2, those that interacted favourably with nutlin (**Fig.** 7). These were, as expected, hydrophobic residues. In order to preserve the fold of MDM2, we explored mutations that replaced these residues with other hydrophobic residues. The mutations examined were: L54W, L54M, L54I, L54F, L57W, L57M, L57I, L57F, I61L, I61M, I61F, I61W, F86I, F86L, F86M and F86W. Out of these, we found two mutations (L57F and L57W, **Table ST2, Fig. 12**), which appear to stabilize interactions with p53 (marginally) and destabilize interactions with nutlin (binding energies reduce by ~4–9 kcal/mol). The Leu57 sidechain is in the binding pocket of MDM2 and is localized in the Trp binding pocket. The structural models suggest that the p53 Trp23 can stack against the Trp57 sidechain of MDM2 without disrupting binding; in contrast, Trp57 sidechain pushes nutlin out of the binding pocket. Further, our calculations also show that G58W, G58L, G58M could be gain of function mutations (they increase the binding affinity for p53 by 2–4 kcal/mol relative to wild type). In addition, the energetic contributions of individual residues to the binding of p53 (**Fig. 7A and B**) provide clues to hypothesize the second class of mutations. These may arise at positions such as D46, E52 whereby charge-removing mutations may (a) change the flexibility of MDM2 (b) increase the affinity for p53 through electrostatics without any change in affinity for nutlin; a similar feature has been reported for mutations in the EGFR kinases whereby certain mutations thought to destabilize drug binding were found to do so by increasing their affinities for ATP.[72] It is interesting that upon browsing the UNIPROT database of MDM2 sequences, we did come across 4 sequences (Q9H4C4, Q9H4C5, Q546E6 and Q8TE46 from soft-tissue sarcoma[73,74]) that have the mutations D46S and E52I,

both of which remove the negative-charge induced destabilization of p53 binding.

We have not carried out analogous computations for MDMX; however we could hypothesize that MDMX could possibly mutate in the N-terminal domain to become more MDM2-like since the latter will bind p53 tighter, thus leading to a gain of function phenotype (for example, Met53 → Leu; Ile99 → Leu; Ser96 → Arg; this will have the additional ability to bind tighter to p53 due to enhanced charge-charge interactions). We eagerly await data from sequencing of tumors to see if our hypothesis and methodology can be extended to predictions of this class of mutations.

Materials and Methods

The initial structure of MDM2-p53 was taken from the crystal structure of p53 bound to MDM2 (PDB code 1YCR, resolved at 2.6 Å[66]); the structure of nutlin (Nutlin2) was taken from the structure of MDM2 complexed with nutlin (PDB code 1RV1, resolved at 2.3 Å[28]) and modelled on to the structure of MDM2 taken from the crystal structure 1YCR (1RV1 contains a mutation, L33E in MDM2). The initial structure of MDMX-p53 was taken from the crystal structure of p53 bound to MDMX (PDB code 3DAB, resolved at 1.9 Å[50]); and the structure of p53 used with MDMX was taken from 1YCR since the p53 used in 3DAB was shorter in length. Nutlin was modelled using 1RV1 as for MDM2. The structures used included residues 25–109 of human MDM2, residues 23–109 of human MDMX and residues 17–29 of human p53. The N- and C-termini of MDM2 were capped with acetyl (ACE) and N-methyl (NME) respectively to keep them neutral; the N-terminii of p53 peptides were capped with ACE. Molecular dynamics simulations were performed with the SANDER module of the AMBER8,[75] package employing the all-atom Cornell force field.[76] Nutlin parameters were built using antechamber.[77,78] Simulations were carried out for the complexes of p53-MDM2, nutlin-MDM2, p53-MDMX and nutlin-MDMX. In addition, simulations were also carried out for the uncomplexed proteins, peptide and nutlin separately. Each system was solvated with a TIP3P water box[79] whose sides are at a minimum distance of 8 Å to any protein atom. Particle Mesh Ewald method (PME)[80] was used for treating the long range electrostatics. All bonds involving hydrogen were constrained by SHAKE.[81] A time step of 2fs used for the integration. Initially, the whole system was minimized for 4,000 steps, to remove any unfavourable interactions. Subsequently, the systems were each heated to 300 K for 75 ps under NPT conditions. After this, each system was simulated for 15 ns at constant temperature (300 K) and pressure (1 atm) and structures were stored every 1 ps. The free energy of binding (ΔG_{bind}) of the peptides to MDM2 was computed using the MM-GBSA (molecular mechanics/Generalized Born surface area) method[82,83] using the GB module[84] in Amber while the non-polar component was estimated from the solvent accessible surface area using MOLSURF[85] using: $\Delta G_{solv,np}$ = 0.00542*SASA + 0.92.[86] Each energy term was averaged over frames taken every 2 ps from the simulation. Vibrational entropy was estimated using normal mode analysis (Nmode module of Amber)[87] and averaged over 200 ps intervals. Electrostatic calculations were done using APBS.[88] PyMOL[89] and Visual Molecular Dynamics[90] (VMD) were used for visualizations. Scwrl[91] was used for side chain refinement of mutations.

Acknowledgements

BII and the p53 lab are funded by BMRC, A-STAR, Singapore. C.V. is adjunct at DBS (NUS) and SBS (NTU); D.P.L. is adjunct at NUS. We thank Jagadeesh, Shubhra and Devan for useful discussions.

Note

Supplementary materials can be found at:
www.landesbioscience.com/supplement/JosephCC9-6-Sup.pdf

References

1. Lane DP. Cancer. p53, guardian of the genome. Nature 1992; 358:15-6.
2. Harris CC. p53 tumor suppressor gene: from the basic research laboratory to the clinic—an abridged historical perspective. Carcinogenesis 1996; 17:1187-98.
3. El-Deiry W. Regulation of p53 downstream genes. Seminars Cancer Biol 1998; 8:345-57.
4. Maya R, Kazaz A, Oren M. Mdm2 promotes the rapid degradation of p53. Nature 1997; 387:296-9.
5. Shimizu H, Burch LR, Smith AJ, Dornan D, Wallace M, Ball KL, et al. The conformationally flexible S9-S10 linker region in the core domain of p53 contains a novel MDM2 binding site whose mutation increases ubiquitination of p53 in vivo. J Biol Chem 2002; 277:28446-58.
6. Candeias MM, Malbert-Colas L, Powell DJ, Daskalogianni C, Maslon MM, Naski N, et al. p53 mRNA controls p53 activity by managing Mdm2 functions. Nat Cell Biol 2008; 10:1098-105.
7. Naski N, Gajjar M, Bourougaa K, Malbert-Colas L, Fåhraeus R, Candeias MM. The p53 mRNA-Mdm2 interaction. Cell Cycle 2009; 8:31-4.
8. Oliner JD, Kinzler KW, Meltzer PS, George DL, Vogelstein B. Amplification of a gene encoding a p53-associated protein in human sarcomas. Nature 1992; 358:80-3.
9. Marchetti A, Buttitta F, Girlando S, Dalla Palma P, Pellegrini S, Fina P, et al. Mdm2 gene alterations and mdm2 protein expression in breast carcinomas. J Pathol 1995; 175:31-8.
10. Reifenberger G, Liu L, Ichimura K, Schmidt EE, Collins VP. Amplification and overexpression of the MDM2 gene in a subset of human malignant gliomas without p53 mutations. Cancer Res 1993; 53:2736-9.
11. Blueso-Ramos CE, Yang Y, deLeon E, McCown P, Stass SA, Albitar M. The human MDM-2 oncogene is overexpressed in leukemias. Blood 1993; 82:2617-23.
12. Shvarts A, Steegenga WT, Riteco N, van Laar T, Dekker P, Bazuine M, et al. MDMX: a novel p53-binding protein with some functional properties of MDM2. EMBO J 1996; 15:5349-57.
13. Marine JC, Jochemsen AG. Mdmx as an essential regulator of p53 activity. Biochem Biophys Res Commun 2005; 331:750-60.
14. Linares LK, Hengstermann A, Ciechanover A, Müller S, Scheffner M. HdmX stimulates Hdm2-mediated ubiquitination and degradation of p53. Proc Natl Acad Sci USA 2003; 100:12009-14.
15. Poyurovsky MV, Priest C, Kentsis A, Borden KL, Pan ZQ, Pavletich N, et al. The Mdm2 RING domain C-terminus is required for supramolecular assembly and ubiquitin ligase activity. EMBO J 2007; 26:90-101.
16. Uldrijan S, Pannekoek WJ, Vousden KH. An essential function of the extreme C-terminus of MDM2 can be provided by MDMX. EMBO J 2007; 26:102-12.
17. Bottger V, Bottger A, Garcia-Echeverria C, Ramos YF, van der Eb AJ, Jochemsen AG, et al. Comparative study of the p53-mdm2 and p53-MDMX interfaces. Oncogene 1999; 18:189-99.
18. Lee HJ, Srinivasan D, Coomber D, Lane DP, Verma CS. Modulation of the p53-MDM2 interaction by phosphorylation of Thr18: a computational study. Cell Cycle 2007; 6:2604-11.
19. Dastidar SG, Lane DP, Verma CS. Multiple peptide conformations give rise to similar binding affinities: molecular simulations of p53-MDM2. J Am Chem Soc 2008; 130:13514-5.
20. Zhong H, Carlson HA. Computational studies and peptidomimetic design for the human p53-MDM2 complex. Proteins 2005; 58:222-34.
21. Grässlin A, Amoreira C, Baldridge KK, Robinson JA. Thermodynamic and Computational Studies on the Binding of p53-Derived Peptides and Peptidomimetic Inhibitors to HDM2. Chembiochem 2009; 10:1360-8.
22. Xia M, Knezevic D, Tovar C, Huang B, Heimbrook DC, Vassilev LT. Elevated MDM2 boosts the apoptotic activity of p53-MDM2 binding inhibitors by facilitating MDMX degradation. Cell Cycle 2008; 7:1604-12.
23. Ramos YF, Stad R, Attema J, Peltenburg LT, van der Eb AJ, Jochemsen AG. Aberrant expression of HDMX proteins in tumor cells correlates with wild-type p53. Cancer Res 2001; 61:1839-42.

24. Hu B, Gilkes DM, Chen J. Efficient p53 activation and apoptosis by simultaneous disruption of binding to MDM2 and MDMX. Cancer Res 2007; 67:8810-7.
25. Hu B, Gilkes DM, Farooqi B, Sebti SM, Chen J. MDMX overexpression prevents P53 activation by the MDM2 inhibitor nutlin. J Biol Chem 2006; 281:33030-5.
26. Laurie NA, Donovan SL, Shih CS, Zhang J, Mills N, Fuller C, et al. Inactivation of the p53 pathway in retinoblastoma. Nature 2006; 444:61-6.
27. Wade M, Wahl GM. Targeting Mdm2 and Mdmx in cancer therapy: better living through medicinal chemistry? Mol Cancer Res 2009; 7:1-11.
28. Vassilev LT, Vu BT, Graves B, Carvajal D, Podlaski F, Filipovic Z, et al. In vivo activation of the p53 pathway by small-molecule antagonists of MDM2. Science 2004; 303:844-8.
29. Shangary S, Qin D, McEachern D, Liu M, Miller RS, Qiu S, et al. Temporal activation of p53 by a specific MDM2 inhibitor is selectively toxic to tumors and leads to complete tumor growth inhibition. Proc Natl Acad Sci USA 2008; 105:3933-8.
30. Pazgier M, Liu M, Zou G, Yuan W, Li C, Li C, et al. Structural basis for high-affinity peptide inhibition of p53 interactions with MDM2 and MDMX. Proc Natl Acad Sci USA 2009; 106:4665-70.
31. Harker EA, Daniels DS, Guarracino DA, Schepartz A. Beta-peptides with improved affinity for hDM2 and hDMX. Bioorg Med Chem 2009; 17:2038-46.
32. Madhumalar A, Lee HJ, Brown CJ, Lane DP, Verma CS. Design of a novel MDM2 binding peptide based on the p53 family. Cell Cycle 2009; 8:2828-36.
33. Robinson JA. Beta-hairpin peptidomimetics: design, structures and biological activities. Acc Chem Res 2008; 41:1278-88.
34. Michel J, Harker EA, Tirado-Rives J, Jorgensen WL, Schepartz A. In Silico Improvement of beta3-peptide inhibitors of p53 x hDM2 and p53 x hDMX. J Am Chem Soc 2009; 131:6356-7.
35. Sakurai K, Schubert C, Kahne D. Crystallographic analysis of an 8-mer p53 peptide analogue complexed with MDM2. J Am Chem Soc 2006; 128:11000-1.
36. Czarna A, Popowicz GM, Pecak A, Wolf S, Dubin G, Holak TA. High affinity interaction of the p53 peptide-analogue with human Mdm2 and Mdmx. Cell Cycle 2009; 8:1176-84.
37. llen J, Goepfert A, Blechschmidt A, Izaac A, Geiser M, Tavares G, et al. Crystal Structures of Human MdmX (HdmX) in Complex with p53 Peptide Analogues Reveal Surprising Conformational Changes. J Biol Chem 2009; 284:8812-21.
38. Patton JT, Mayo LD, Singhi AD, Gudkov AV, Stark GR, Jackson MW. Levels of HdmX expression dictate the sensitivity of normal and transformed cells to Nutlin-3. Cancer Res 2006; 66:3169-76.
39. Boehr DD, Nussinov R, Wright PE. The role of dynamic conformational ensembles in biomolecular recognition. Nat Chem Biol 2009; 5:789-96.
40. Schames JR, Henchman RH, Siegel JS, Sotriffer CA, Ni H, McCammon JA. Discovery of a novel binding trench in HIV integrase. J Med Chem 2004; 47:1879-81.
41. Rutherford K, Daggett V. The V119I polymorphism in protein L-isoaspartate O-methyltransferase alters the substrate-binding interface. Protein Eng Des Sel 2009; 22:713-21.
42. Dodson GG, Lane DP, Verma CS. Molecular simulations of protein dynamics: new windows on mechanisms in biology. EMBO Rep 2008; 9:144-50.
43. Ding Y, Mei Y, Zhang JZ. Quantum mechanical studies of residue specific hydrophobic interactions in p53-MDM2 binding. J Phys Chem B 2008; 112:11396-401.
44. Espinoza-Fonseca LM, Garcia-Machorro J. Aromatic-aromatic interactions in the formation of the MDM2-p53 complex. Biochem Biophys Res Commun 2008; 370:547-51.
45. Chen HF, Luo R. Binding induced folding in p53-MDM2 complex. J Am Chem Soc 2007; 129:2930-7.
46. Espinoza-Fonseca LM, Trujillo-Ferrara JG. Conformational changes of the p53-binding cleft of MDM2 revealed by molecular dynamics simulations. Biopolymers 2006; 83:365-73.
47. Massova I, Kollman PA. Computational Alanine scanning to probe protein-protein interactions: A novel approach to evaluate binding free energies. J Am Chem Soc 1999; 121:8133-43.
48. Carotti A, Macchiarulo A, Giacchè N, Pellicciari R. Targeting the conformational transitions of MDM2 and MDMX: Insights into key residues affecting p53 recognition. Proteins 2005; 77:524-35.
49. Macchiarulo A, Giacchè N, Carotti A, Baroni M, Cruciani G, Pellicciari R. Targeting the conformational transitions of MDM2 and MDMX: insights into dissimilarities and similarities of p53 recognition. J Chem Inf Model 2008; 48:1999-2009.
50. Popowicz GM, Czarna A, Holak TA. Structure of the human Mdmx protein bound to the p53 tumor suppressor transactivation domain. Cell Cycle 2008; 7:2441-3.
51. Terzian T, Suh YA, Iwakuma T, Post SM, Neumann M, Lang GA, et al. The inherent instability of mutant p53 is alleviated by Mdm2 or $p16^{INK4a}$ loss. Genes Dev 2008; 22:1337-44.
52. Li Y, Prives C. Are interactions with p63 and p73 involved in mutant p53 gain of oncogenic function? Oncogene 2007; 26:2220-5.
53. Vousden KH. Functions of p53 in metabolism and invasion. Biochem Soc Trans 2009; 37:511-7.
54. Amadei A, Linssen AB, Berendsen HJ. Essential dynamics of proteins. Proteins 1993; 4:412-25.
55. Hayward S, Kitao A, Go N. Harmonicity and anharmonicity in protein dynamics: a normal mode analysis and principal component analysis. Proteins 1995; 23:177-86.
56. Hayward S, Kitao A, Hirata F, Go N. Effect of solvent on collective motions in globular protein. J Mol Biol 1993; 234:1207-17.
57. Hayward S, Kitao A, Go N. Harmonic and anharmonic aspects in the dynamics of BPTI: a normal mode analysis and principal component analysis. Protein Sci 1994; 3:936-43.
58. Lee H, Mok KH, Muhandiram R, Park KH, Suk JE, Kim DH, et al. Local structural elements in the mostly unstructured transcriptional activation domain of human p53. J Biol Chem 2000; 275:29426-32.
59. Jagadeesh MN, Madhumalar A, Beuerman RW, Lane DP, Verma CS. Differences in the transactivation domains of p53 family members: a computational study. BMC genomics 2009; (In Press).
60. Schon O, Friedler A, Bycroft M, Freund SMV, Fersht AR. Molecular mechanism of the interaction between MDM2 and p53. J Mol Biol 2002; 323:491-501.
61. Bottger A, Bottger V, Garcia-Echeverria C, Chene P, Hochkeppel H, Sampson W, et al. Molecular characterization of the HDM2-p53 interaction. J Mol Biol 1997; 269:744-76.
62. Fischer S, Verma CS, Hubbard RE. Rotation of structural water inside a protein: calculation of the rate and vibrational entropy of activation. J Phys Chem B 1998; 102:1797-805.
63. Fischer S, Verma CS. Binding of buried structural water increases the flexibility of proteins. Proc Natl Acad Sci USA 1999; 96:9613-5.
64. Madhumalar A, Smith DJ, Verma C. Stability of the core domain of p53: insights from computer simulations. BMC Bioinformatics 2008; 9:17.
65. Kallen J, Goepfert A, Blechschmidt A, Izaac A, Geiser M, Tavares G, et al. Crystal Structures of Human MdmX (HdmX) in Complex with p53 Peptide Analogues Reveal Surprising Conformational Changes. J Biol Chem 2009; 284:8812-21.
66. Kussie PH, Gorina S, Marechal V, Elenbaas B, Moreau J, Levine AJ, et al. Structure of the MDM2 oncoprotein bound to the p53 tumor supressor transactivation domain. Science 1996; 274:948-53.
67. Ohtaka H, Freire E. Adaptive inhibitors of the HIV-1 protease. Prog Biophys Mol Biol 2005; 88:193-208.
68. Balius TE, Rizzo RC. Quantitative prediction of fold resistance for inhibitors of EGFR. Biochemistry 2009; 48:8435-48.
69. Freedman DA, Epstein CB, Roth JC, Levine AJ. A genetic approach to mapping the p53 binding site in the MDM2 protein. Mol Med 1997; 3:248-59.
70. Mendes J, Baptista AM, Carrondo MA, Soares CM. Improved modeling of side-chains in proteins with rotamer-based methods: a flexible rotamer model. Proteins 1999 37:530-43.
71. Bower MJ, Cohen FE, Dunbrack RL Jr. Prediction of protein side-chain rotamers from a backbone-dependent rotamer library: a new homology modeling tool. J Mol Biol 1997 267:1268-82.
72. Yun CH, Mengwasser KE, Toms AV, Woo MS, Greulich H, Wong KK, et al. The T790M mutation in EGFR kinase causes drug resistance by increasing the affinity for ATP. Proc Natl Acad Sci USA 2008; 105:2070-5.
73. Bartel F, Meye A, Wurl P, Kappler M, Bache M, Lautenschlager C, et al. Amplification of the MDM2 gene, but not expression of splice variants of MDM2 MRNA, is associated with prognosis in soft tissue sarcoma Int J Cancer 2001; 95:168-75.
74. Taubert H, Kappler M, Meye A, Bartel F, Schlott T, Lautenschläger C, et al. A MboII polymorphism in exon 11 of the human MDM2 gene occuring in normal blood donors and in soft tissue sarcoma patients: an indication for an increased cancer susceptibility? Mutat Res 2000; 456:39-44.
75. Case DA, Darden TA, Cheatham TE, Simmerling CL, Wang J, Duke RE, et al. AMBER8. San Francisco: University of California 2004.
76. Cornell WD, Cieplak P, Bayly CI, Gould IR, Merz KM, Ferguson DM, et al. A second-generation force field for the simulation of proteins, nucleic acids and organic molecules. J Am Chem Soc 1995; 117:5179-97.
77. Wang J, Wolf RM, Caldwell JW, Kollman PA, Case DA, Development and testing of a general AMBER force field. J Comput Chem 2004; 25:1157-74.
78. Wang J, Wang W, Kollman PA, Case DA, Automatic atom type and bond type perception in molecular mechanical calculations. J Mol Graph Model 2006; 25:247-60.
79. Jorgensen WL, Chandrasekhar J, Madura JD, Impey RW, Klein ML. Comparison of simple potential functions for simulating liquid water. J Chem Phys 1983; 79:926-35.
80. Darden T, York D, Pedersen L. Particle mesh Ewald: An N.log(N) method for Ewald sums in large systems. J Chem Phys 1993; 98:10089-92.
81. van Gunsteren WF, Berendsen HJC. Algorithms for macromolecular dynamics and constraint dynamics. Mol Phys 1977; 34:1311-27.
82. Bashford D, Case DA. Generalized Born models of macromolecular solvation effects. Annu Rev Phys Chem 2000; 51:129-52.
83. Tsui V, Case DA. Molecular dynamics simulations of nucleic acids with a Generalized Born solvation model. J Am Chem Soc 2000; 122:2489-98.
84. Jayaram B, Sprous D, Beveridge DL. Solvation free energy of biomacromolecules: Parameters for a modified Generalized Born model consistent with the AMBER force field. J Phys Chem B 1998; 102:9571-6.
85. Connolly ML. Solvent-accessible surfaces of proteins and nucleic acids. Science 1983; 221:709-13.
86. Sanner MF, Olson AJ, Spehner JC. Reduced surface: An efficient way to compute molecular surfaces. Biopolymers 1996; 38:305-20.
87. Case DA. Normal-mode analysis of protein dynamics. Curr Opin Struct Biol 1994; 4:285-90.
88. Baker NA, Sept D, Joseph S, Holst MJ, McCammon JA. Electrostatics of nanosystems: Application to microtubules and the ribosome. Proc Natl Acad Sci USA 2001; 98:10037-41.
89. DeLano WL. The PyMOL molecular graphics system. San Carlos CA, USA: DeLano Scientific 2002.
90. Humphrey W, Dalke A, Schulten K. VMD-visual molecular dynamics. J Mol Graph 1996; 14:33-8.
91. Canutescu AA, Shelenkov AA, Dunbrack RL Jr. A graph-theory algorithm for rapid protein side-chain prediction. Protein Sci 2003; 12:2001-14.